Ore Geology Reviews 92 (2018) 240–256

Contents lists available at ScienceDirect

Ore Geology Reviews

journal homepage: www.elsevier.com/locate/oregeorev

3D characteristic analysis-based targeting of concealed Kiruna-type Fe oxide-apatite mineralization within the Yangzhuang deposit of the Zhonggu orefield, southern Ningwu volcanic basin, middle-lower Yangtze River metallogenic Belt, China

Xunyu Hu[a,b], Feng Yuan[a,b,c,*], Xiaohui Li[a,b], Simon M. Jowitt[d], Cai Jia[a,b], Mingming Zhang[a,b], Taofa Zhou[a,b]

[a] School of Resources and Environmental Engineering, Hefei University of Technology, Hefei 230009, China
[b] Anhui Province Engineering Research Center for Mineral Resources and Mine Environments, Hefei University of Technology, Hefei, Anhui 230009, China
[c] Xinjiang Research Centre for Mineral Resources, Xinjiang Institute of Ecology and Geography, Chinese Academy of Sciences, Urumqi, Xinjiang 830011, China
[d] Department of Geoscience, University of Nevada Las Vegas, Las Vegas, 4505 S. Maryland Pkwy., NV 89154-4010, USA

ARTICLE INFO

Keywords:
3D geological modeling
3D spatial analysis
Characteristic analysis
Prospectivity modeling
Yangzhuang deposit

ABSTRACT

The computer-based modeling of geological and geophysical data allows the construction of 3D geological models that can predict the location of differing lithologies, intrusive units and orebodies. This 3D modeling allows the identification and quantification of the 3D controls on the location and grade and tonnage of mineralization in a given mineral deposit. These controls include factors such as the spatial relationship between mineralization and distinct geological units or features and the record of tectonic movements in an area such as the uplifting or subsidence of individual rock masses during faulting or intrusion. These controls on mineralization can then be combined with the location of areas of known mineralization in an approach termed characteristic analysis, which allows the identification of areas that are prospective for previously unknown mineralization as well as the 3D targeting of areas for future mineral exploration. Here, we present a case study that focuses on the Yangzhuang deposit within the Zhonggu orefield of the southern Ningwu volcanic basin, an important mineral deposit within the middle-lower Yangtze River Metallogenic Belt, China. This case study uses the 3D metallogenic prospectivity modeling approach outlined above. Our research indicates that areas of known mineralization (i.e., already identified orebodies) can be used to train 3D datasets to identify areas that are highly prospective for future exploration, in this case a highly prospective region to the north-northeast of the known mineralization in this area. This region is coincident with a distinct magnetic anomaly, suggesting that this area is likely to host significant mineralization, a hypothesis that will be tested during future exploration. This study outlines an approach to 3D prospectivity modeling that can be used in both greenfield and brownfield exploration and provides a new method for the exploration targeting of concealed or deep mineralization, representing a significant advance over the more widely used 2D prospectivity modeling techniques.

1. Introduction

Mineral exploration has become more difficult over time, primarily as outcropping and near-surface mineralization is more easily identified and exploited than concealed or deep-seated and unexposed mineralization. This in turn means that identifying prospective areas during exploration targeting has also become more difficult over time. As such, mineral exploration is generally facing a situation where mineralization is hard to recognize, hard to discover, hard to exploit, a dilemma that can be overcome by targeting deep and peripheral but unexposed sections of existing deposits during brownfield exploration and the required expansion of the resources and reserves of existing mines. This type of approach is vital in order to keep operations running and to extend the life span of individual mines (e.g., Zhao and Chen, 2000). A subset of recent exploration targeting research has focused on the development of mathematical geological approaches (Zhao, 2003; Mao et al., 2011; Chen et al., 2007, 2009; Li et al., 2014; Porwal and Carranza, 2015), although deep-seated and unexposed mineralization is usually associated with very weak or negligible surface anomalies and may be associated with areas of mining activity that have disturbed the

* Corresponding author at: School of Resources and Environmental Engineering, Hefei University of Technology, Hefei 230009, China.
E-mail address: yf_hfut@163.com (F. Yuan).

https://doi.org/10.1016/j.oregeorev.2017.11.019
Received 10 July 2016; Received in revised form 14 November 2017; Accepted 22 November 2017
Available online 23 November 2017
0169-1368/

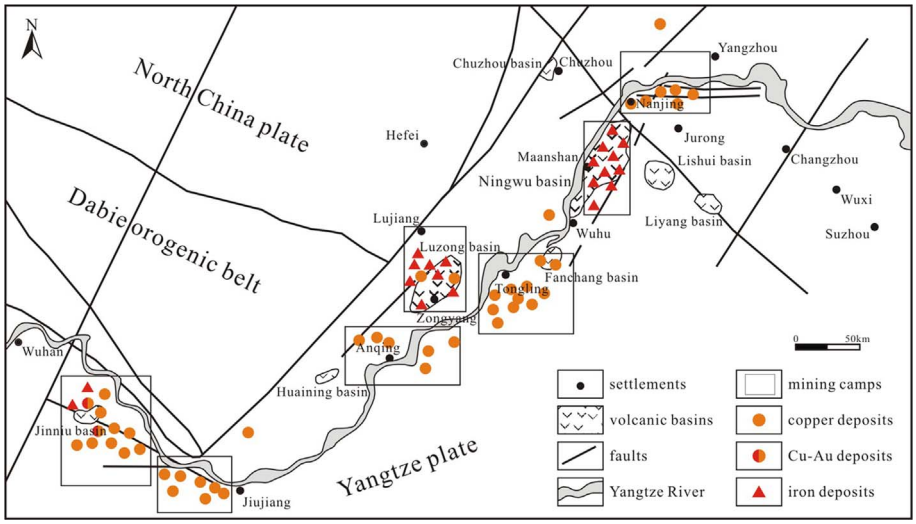

Fig. 1. Map showing the location of major volcanic basins within the middle and lower Yangtze River valley. Modified after Zhai (1992).

natural geological, geophysical and geochemical anomalies that are associated with mineralization. This in turn means that the areas around known orebodies may be lacking in precise and accurate geological and geophysical data that reflects the natural geology of the area but instead may have been anthropogenically disturbed or may be occluded by barren units within the same area. One solution to this issue is 3D prospectivity modeling, a rapidly developing sector of prospectivity modeling that provides new ideas and approaches to the problems encountered during mineral exploration (Zhao, 2003; Mao et al., 2011, 2016; Chen et al., 2007, 2009; Li et al., 2014; Yuan et al., 2014a, b; Zhang, 2014). Traditional approaches typically use various mathematical methods during resource assessment and prospectivity modeling, including prospectivity content modeling (Zhao, 1983; Chen et al., 2008), Boolean logic and index superposition based methods (Bonham-Carter, 1994), weight of evidence-based methods (Bonham-Carter et al., 1989; Agterberg et al., 1993; Zhang et al., 2009; Wang, 2012), logistic regression based methods (Agterberg et al., 1993; Porwal et al., 2010), artificial neural network based methods (Li et al., 2014; Brown et al., 2000), fuzzy logic based and fuzzy inference system based models (Joly et al., 2012; Porwal et al., 2015) and characteristic analysis methods (Ni and Xue, 2007; Zhang et al., 2012; Wu et al., 2015). The latter has been extensively used for 2D surficial prospectivity modeling where the characteristics of known mineralization are used to train data to identify prospective areas for future mineral exploration. The characteristics analysis methodology is designed to deal with geochemical variables at the beginning and focuses on measured values that differ locally from neighboring locations and on correlations between variables based on a small number of observations (Botbol et al., 1977). It also requires minimal calculations, which makes the method easy to implement. However, this approach has not been used in 3D prospectivity modeling before this study. This study represents an attempt to apply characteristics analysis method to our study area, the Yangzhuang deposit, and compares the results obtained using this method and the more traditional weights of evidence approach to test the effectiveness of the former. We use a significant amount of data obtained for the research area, making this an ideal location with sufficient specific characteristics for the application of the characteristics analysis method, assuming that areas with similar geological characteristics contain similar amounts of mineralization. All of this means that characteristics analysis is ideally suited for use in the generation of a 3D prospectivity model for this region.

Here, we present a case study of 3D characteristic analysis-based prospectivity modeling for the targeting of mineralization associated with the Kiruna-type iron oxide-apatite type Yangzhuang iron deposit within the Zhonggu orefield of in the southern Ningwu volcanic basin (Jin, 2014; Ningwu Research Group, 1978). This area is well characterized, primarily as a result of the significant amount of legacy geological data generated during previous exploration in this region (Ningwu Research Group, 1978; East China Mineral Exploration and Development Bureau, 2011; Li et al., 2015). The proliferation of existing data for this area allows the construction of prospectivity models for the deeper and peripheral portions of the main Yangzhuang orebody, an approach that then allows this 3D modeling to be linked with regional geological structures and features to identify deep-seated or distal areas that are prospective for future exploration. As such, this combination of 3D geological modeling, 3D spatial analysis and 3D characteristics analysis allows the generation of a 3D prospectivity model for the deep and peripheral regions of the main Yangzhuang orebody. The results of this approach were verified by comparison to areas of known mineralization, ensuring that this approach to exploration for deep and concealed mineralization yields the best chance of exploration success both in the study area and elsewhere where this technique could be applied. We also used the same 3D geological model and the data obtained from the 3D spatial analysis to run a weights of evidence model, allowing the direct comparison of these two methods. Our results indicate that the characteristics analysis based approach is more effective for guiding future exploration around the Yangzhuang iron deposit than the more commonly used weights of evidence method.

2. Geology of the study area

2.1. Regional geology

The middle and lower Yangtze River Metallogenic Belt (MLYRMB; Fig. 1) hosts world-class Cu–Fe polymetallic mineralization and is one of the most important areas of mineralization in China (Ningwu Research Group, 1978; Tang, 1998; Chang, 1991; Zhai, 1992). The area is cross-cut by a series of major faults and hosts seven large mining camps, namely the southeast Hubei, Jiurui, Anqing–Guichi, Luzong, Tongling, Ningwu, and Ningzhen mining districts (all the mining camps are listed from west to east according to the location in Fig. 1) (Chang, 1991; Yuan etal., 2011; Zhai, 1992; Zhao and Tu, 2003; Zhou et al., 2011). These areas contain mineralization that is generally hosted by the Ningwu and Luzong volcanic basins, the two largest volcanic basins in this region (Zhou et al., 2011). The majority of the basins in the MLYRMB are pull-apart basins that trend N–S to NE–SW, host a series of intrusive and extrusive olivine–latite units and are associated with volcanic–subvolcanic hydrothermal–sedimentary polymetallic iron deposits that are similar to the Kiruna-type Fe oxide–apatite deposits of northern Sweden, in addition to numerous other non-metallic mineral

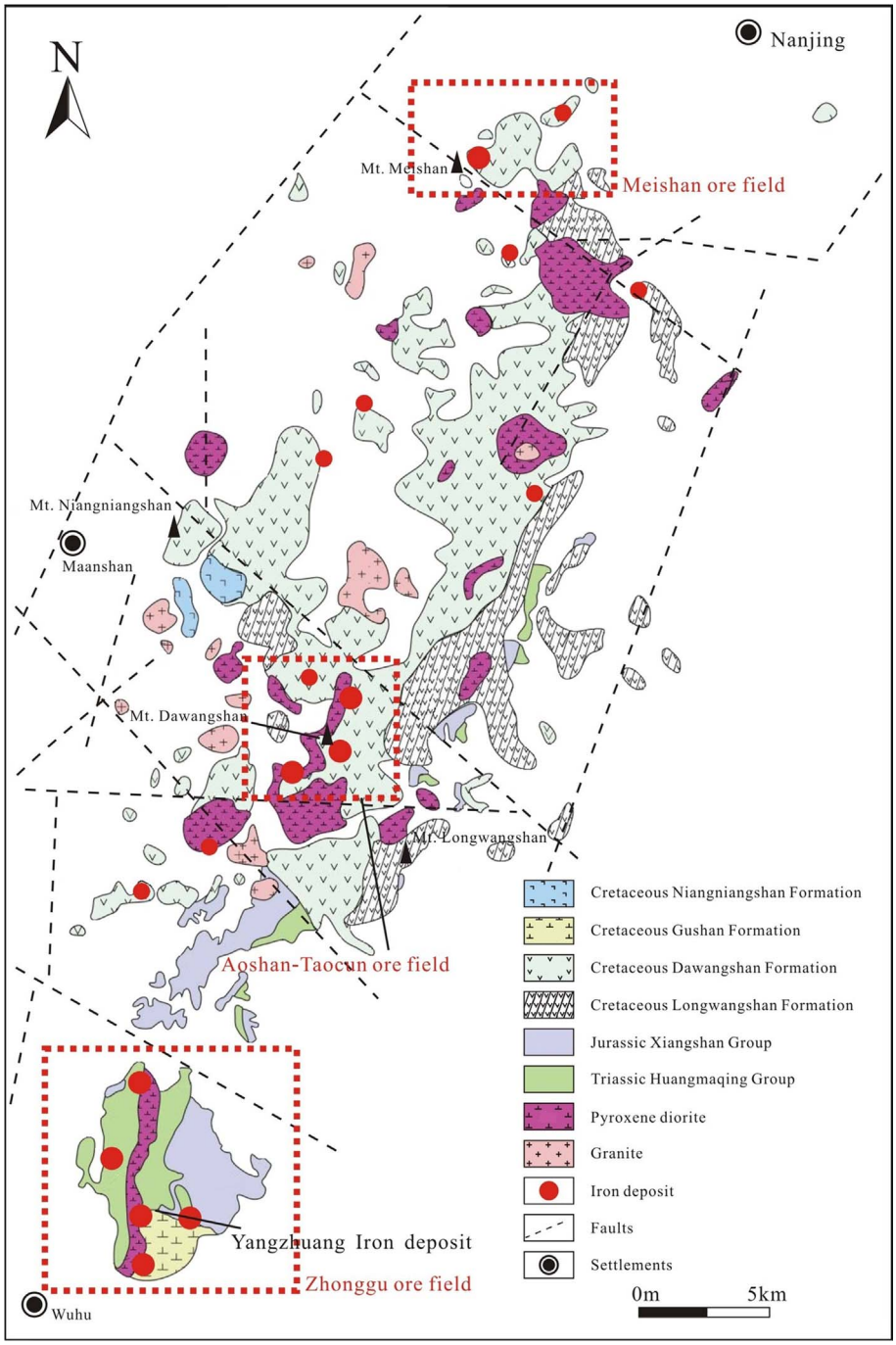

Fig. 2. Map showing the geology and main mineral deposits of the Ningwu Basin Ningwu Research Group (1978).

deposits (Ningwu Research Group, 1978).

The Ningwu basin is located within the eastern MLYRMB and is controlled by two groups of faults that form the tectonic framework of this area, one trending NNE–SSW and the other trending NW–SE. The NNE–SSW trending faults consist of the Yangtze and Fangshan–Nanling faults, whereas the NW–SE trending faults are dominated by the Nanjing–Hushu fault. The basin hosts a series of volcanic units, including the Triassic Zhouchongcun (T_2z) and Huangmaqing (T_3h) groups and the Jurassic Xiangshan Group ($J_{1\text{-}2}xn^1$). These units are overlain by Mesozoic olivinelatite volcanics associated with the Yanshanian magmatic event that are split into four cycles of volcanism, namely (from oldest to youngest) the Longwangshan, Dawangshan, Gushan and Niangniangshan volcanic cycles (Ningwu Research Group, 1978). The Ningwu basin in this area hosts significant iron mineralization, with individual deposits clustered in (from north to south) the Meishan, Aoshan–Taocun and Zhonggu orefields (Fig. 2).

2.2. Geology of the Zhonggu orefield

The Zhonggu orefield is located in the southern Ningwu basin in an area that records folding and faulting that was contemporaneous with the voluminous magmatism recorded in this region. Both the intrusive and extrusive magmatism and the mineralization in this area were controlled by two basement-penetrating faults, one trending NNE–SSW and the other trending NNW–SSE (Fig. 3). The area is dominated by units of the Triassic Zhouchongcun (T_2z), Triassic Huangmaqing (T_3h) and Jurassic Xiangshan ($J_{1\text{-}2}xn^1$) groups, with the former two units closely associated with the iron mineralization in this region. All of the iron-dominated mineral deposits in this area are associated with small hypabyssal to superhypabyssal intrusions, including the

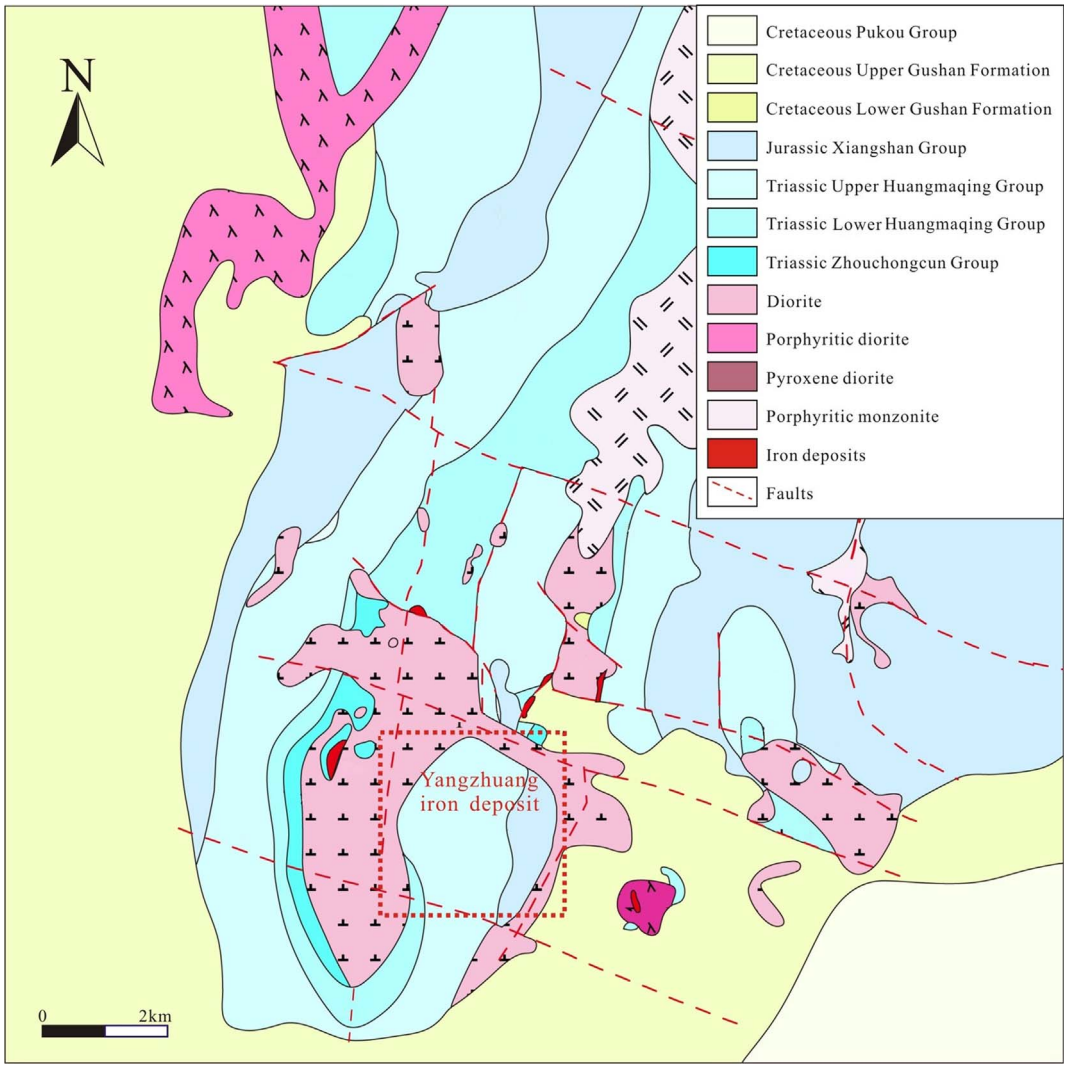

Fig. 3. Map showing the geology and mineral deposits of the Zhonggu orefield adapted from data obtained from the East China Mineral Exploration and Development Bureau.

Yunlou–Hemushan porphyritic diorite, the Zhongjiu porphyritic diorite, the Qingjieshan–Baixiangshan porphyritic diorite, the Gushan–Caogang porphyritic diorite and the Yangzhuang porphyritic diorite (Hou et al., 2010).

2.3. Deposit geology

The Yangzhuang iron deposit is located in the southern part of the Zhonggu orefield and is a Kiruna-type Fe oxide-apatite deposit that was formed as a result of magmato-hydrothermal fluid circulation associated with a porphyritic magmatic intrusion in this area (East China Mineral Exploration and Development Bureau, 2011; Jin, 2014). This area contains Triassic to Quaternary sediments, with the latter covering a significant portion of the region (Fig. 4). Drillholes in this area indicate that the Quaternary sediments in this region cover units that include the Triassic Huangmaqing (T_2h) and Xujiashan (T_2x) and the Jurassic Xiangshan ($J_{1\text{-}2}xn$) groups, with the Xujiashan Group split into the Huangmaqing (T_2h^1) and Zhouchongcun (T_2z) formations. The intrusive unit in this area is controlled by two small domes that together define a large domal structure. One of these small domes is in the southwestern part of the mining area and records uplift to the southwest and subsidence to the northeast, whereas the other dome is in the northeastern part of this area and contains a central portion of uplift that is surrounded by a region that has been downthrown. The vast majority of the mineralization in this area is hosted by a porphyritic diorite that is entirely concealed (i.e., does not crop out at the surface) and formed from mantle-derived magmas (Wang et al., 2001). The contact between this intrusion and the surrounding country rocks (especially the Triassic Huangmaqing Formation) is a key area for mineralization, with areas associated with uplift associated with the intrusion also important hosts for mineralization in this region along with interformational fractures within the Zhouchongcun Formation, and within the intrusion itself (Li et al., 2015). The locations of all of the intrusions in this area are controlled by folding and faulting that formed the conduits for the magmas, generating the cupolas and stocks observed in this region. The doming of units associated with folding in the study area is an important control on mineralization with the main faults located along the SW and NE edges of the deposit (Fig. 3), meaning that they are peripheral to the mineralization in this area and were not directly involved in metallogenesis. The main mineralization-related intrusion is dominated by a porphyritic diorite phase and is associated with more silica-rich porphyritic diorite, porphyritic felsite, spessartine-bearing and gabbroic dikes in the surrounding area. The iron ore within the deposit is dominated by magnetite with minor amounts of hematite, with the individual orebodies that have been identified by drilling and geophysical detection (magnetic anomalies) generally located along the contact between the porphyritic diorite and the Xujiashan Group, within the Xujiashan Group itself, and within the porphyritic diorite.

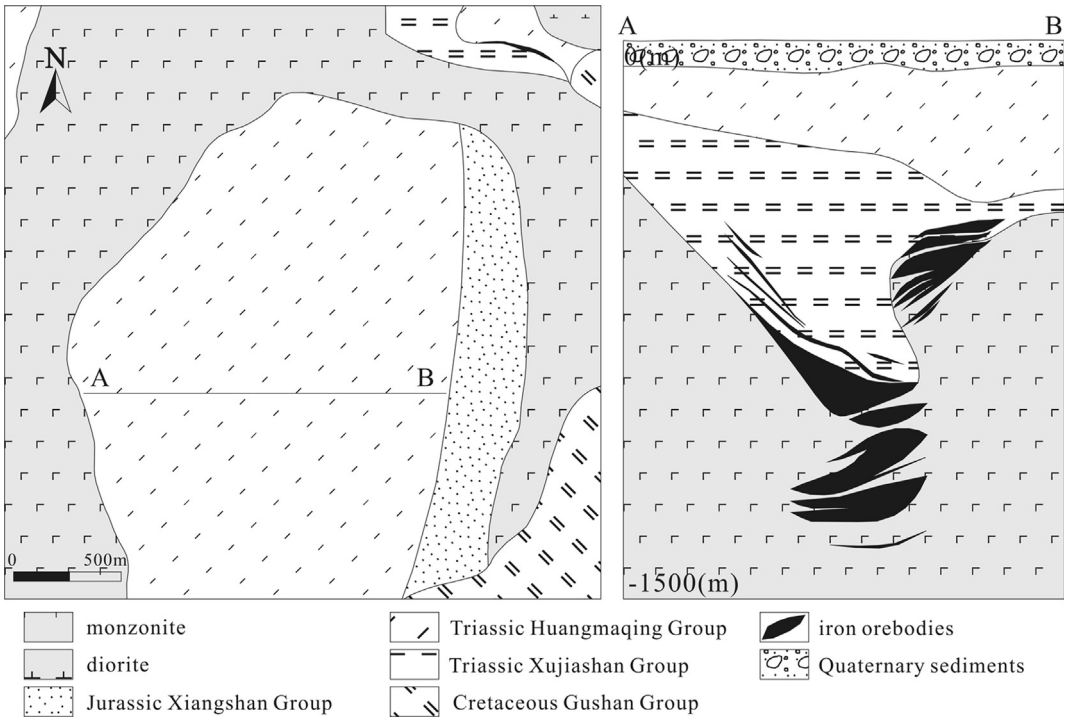

Fig. 4. Map showing the geology of the area around the Yangzhuang iron ore deposit based on data from the East China Nonferrous Geological and Mineral Exploration Development Institute. Modified from East China Mineral Exploration and Development Bureau (2011).

2.4. Dataset and methodology

The structures and contacts within the study area and the 3D models constructed during this study were based on 81 drillhole logs and 10 geological cross-sections (Table 1; Fig. 5).

3. 3D modeling processes and analytical methods

This study uses an approach that combines knowledge of the controls on mineralization in an area with characteristics analysis to generate a 3D prospectivity model for the study area utilizing a .NET based coding approach (Yuan et al., 2014a, b). This approach involves construction of 3D geological models using data obtained from mapping, drillholes, cross-sections and other sources of geological information (e.g., Table 1; Fig. 1). This information is then combined using the above code to enable 3D spatial analysis and the extraction of the controls on mineralization in 3D (i.e., the 3D identification of areas that are prospective for mineralization within individual datasets). These individual datasets are then combined to create a prospectivity model that incorporates all of the factors related to mineralization in the study area using a characteristic analysis method; this workflow is outlined in Fig. 6.

Table 1
Data used during 3D model construction.

Data category	Data size	Data sources
Drillhole logs	81 drillholes transferred into a drillhole database using Surpac™	808 geological team of the East China Mineral Exploration and Development Bureau
Geological cross-sections	10 cross-sections transferred as vector files into Surpac™	808 geological team of the East China Mineral Exploration and Development Bureau

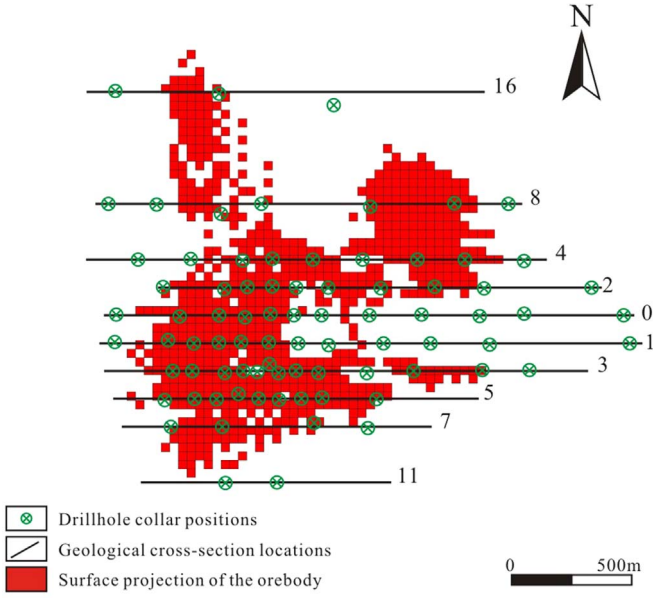

Fig. 5. Map showing the location of data used in the construction of 3D models.

3.1. 3D geological modelling

The 3D approach to geological modelling outlined by Houlding (1994) and used during this study has a general form as follows: a computer generated 3D model is constructed using appropriate software and mathematical modeling to describe geological bodies, structures or some particular characteristics based on geological data. This enables the realization of the 3D positioning and displaying of these bodies, structures or other characteristics from data management, geological interpretation, spatial analysis, geological statistics, prospectivity modeling and 3D visualization (Houlding, 1994; Lv et al., 2011a, b). Current approaches to outline the location and nature of

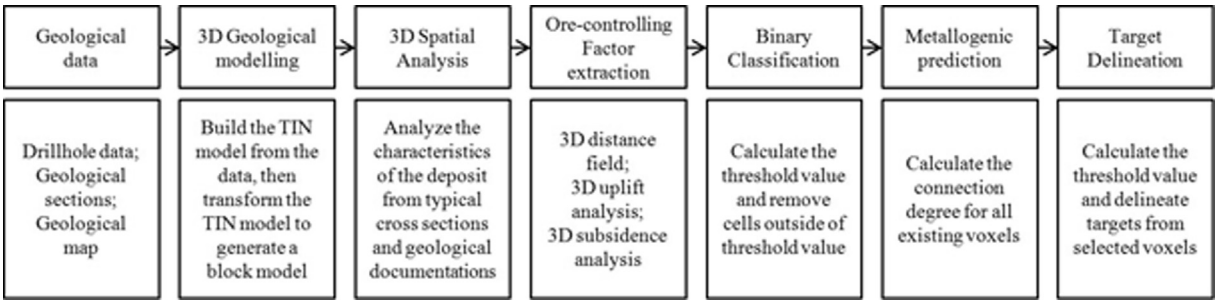

Fig. 6. Workflow used during the 3D prospectivity modeling undertaken during this study.

geological bodies at depth in 3D use mine scale geological data, drillhole-derived data and cross-sections (e.g., Fig. 1; Table 1), 3D inversions generated from gravity and magnetic (Deng et al., 2012) and reflected seismic (Lv et al., 2011a, b) data and synthetic interpreted sections derived from geophysical data (Qi et al., 2012). These 3D models can qualitatively or quantitatively reveal the relationship between adjacent geological bodies, including the volumes of these bodies, the controls on their shapes and forms, and the tectonic history of an area. Further spatial analysis can be used to indirectly obtain information on the controls on mineralization in an area, meaning that these 3D models can be used to identify areas that may host concealed mineralization in areas deeper or peripheral to known mineralization, a key factor in increasing the potential success of mineral exploration.

3.2.1. 3D spatial analysis

The spatial distribution and morphological characteristics of geological bodies and local structures are often controlling factors in the formation and distribution of mineralization in a given area (e.g., Huang, 2013; Jowitt et al., 2014; Mao et al., 2011). Here, we use existing geological data and block models for the Yangzhuang area to undertake Euclidean distance calculations and the analysis of uplift and subsidence associated with both faulting and the intrusion of the porphyritic diorite in the study area.

3.2.2. Euclidean distance calculation

The mineralization within the Yangzhuang deposit is closely associated with the location of key sedimentary units (namely the Xujiashan Group) and the porphyritic diorite in the study area, with this study focusing on these units and the porphyritic diorite itself. The spatial relationships between individual geological bodies and the known volume of mineralization can be determined using Euclidean distance calculations. Correlating the distances between these geological bodies and the location of known mineralization enables the determining of optimal distances (i.e., the distance where the spatial relationship between a given geological unit and known mineralization breaks down) and the construction of 3D volumes that delineate prospective areas relating to the location of individual geological units or bodies. This is undertaken by determining the Euclidean distance between all the blocks within a given model and voxels of known mineralization using the following formula:

$$D(A_1, A_2) = \min \{\sqrt{(x_1-x_2)^2 + (y_1-y_2)^2 + (z_1-z_2)^2}\} \quad (1)$$

where A_1 (x_1, y_1, z_1) and A_2 (x_2, y_2, z_2) are both voxels that have 3D coordinates in the form x, y, z and D is the Euclidean distance between A_1 and A_2 (x, y, z are the coordinates of the center of the voxels). In our calculation process, A_1 (x_1, y_1, z_1) is within the set of known mineralization whereas A_2 (x_2, y_2, z_2) is among the rest of the potentially unmineralized voxels in the 3D model.

3.2.3. 3D uplift and subsidence analysis

Tectonic factors are frequently related to the formation of ore deposits and structures can often control the location of individual volume of mineralization in a given area. Folding can control the location of mineralization with anticlines that formed before or during mineralizing events often hosting mineralization in the form of stratabound or stratiform orebodies or saddle orebodies associated with crush zones on both limbs of a fold (e.g., Chai et al., 2014; Peterson et al., 1976; Song et al., 2015). Folds can also act as conduits or traps for magmatism and hydrothermal fluids, again potentially increasing the likelihood of mineralization being associated with this type of folding (e.g., Vollgger et al., 2015). Faulting can also create conduits for hydrothermal fluids and magmas, and the density of folding and faulting within an individual unit can be analyzed by determining the uplift or subsidence of a given point compared to a stated datum (Yoshinobu et al., 1998; Gall et al., 2000). As such, quantitatively analyzing and extracting the uplift or subsidence of a given geological unit may provide insight into the 3D prospectivity of a given area (we can treat uplift and subsidence as parts of folds or domes; in an area uplift, it's surroundings or two sides must be relatively subsidence, vice versa). The 3D uplift or subsidence of a given voxel of a specific geologic surface (e.g., the contact between the Xujiashan Group and the porphyritic diorite) can be defined by comparing its elevation from the average elevation of the voxel on the surface (Li et al., 2014) using the following formula:

$$L_i = z_i - z_m \quad (2)$$

where L_i is the height of uplift or subsidence of A_i (x_i, y_i, z_i), z_i is the elevation of voxel A_i, and z_m is the average elevation of A_i which is calculated by equalizing elevation of a 5 × 5 matrix centered on A_i (Fig. 7), with L_i values > 0 indicative of the uplift of A_i and L_i values < 0 indicative of subsidence of the same voxel.

The average elevation (z_m) of A_{13} in Fig. 7 is calculated using the following formula where z_i is the elevation of voxel A_i:

A_1	A_2	A_3	A_4	A_5
A_6	A_7	A_8	A_9	A_{10}
A_{11}	A_{12}	A_{13}	A_{14}	A_{15}
A_{16}	A_{17}	A_{18}	A_{19}	A_{20}
A_{21}	A_{22}	A_{23}	A_{24}	A_{25}

Fig. 7. A 5 × 5 matrix centered on A_{13}.

$$z_m = \frac{1}{25}\sum_{i=1}^{25} z_i \tag{3}$$

3.3. 3D prospectivity modeling using characteristic analysis

Characteristic analysis was first proposed as an approach that could effectively interpret regional multivariate geological, geochemical, and geophysical data (Botbol, 1971; Botbol et al., 1977). This approach has been widely using for 2D prospectivity modeling at multiple scales since the 1970s (Botbol, 1971; Botbol et al., 1977; Mccammon et al., 1983; Ni and Xue, 2007; Zhang et al., 2012; Wu et al., 2015) using a method called quantitative similarity analysis. Current prospectivity modeling research through characteristic analysis has generally been focused on 2D surfaces, with comparatively little undertaken in 3D space (e.g., Li et al., 2015). The basic theory of characteristic analysis involves the extraction of one or several characteristics (e.g., faults, geological contacts) from a 3D block model of a given mineral deposit and the analysis of the spatial relationship (positive or negative) between these characteristics and the location of areas of known mineralization. This enables voxels within the model that host mineralization to be given a value that combines these relationships between these characteristics and volume of known mineralization (here termed the value of degree of connection). These values can then be applied to voxels away from areas of known mineralization to identify regions with similar characteristics to those containing known mineralization (i.e., have similar structures, lithologies, or other characteristics that are known to be spatially related to mineralization) that should be considered prospective for future mineral exploration. The prospectivity of all of the voxels within the model is determined using weightings that reflect the differing characteristics of the voxel and the relationships of these characteristics to known mineralization, with these weightings then combined to quantitatively identify areas and delineate targets that are highly prospective for future exploration. The following matrices and formulas are used in this process. Provided that there are m variables x_j ($j = 1, 2, \ldots, m$) and n voxels the x_j value in voxel i is calculated using x_{ij} ($i = 1, 2, \ldots, n$; $j = 1, 2, \ldots, m$), with the original data matrix outlined as follows:

$$X = \begin{bmatrix} x_{11} & x_{12} & \cdots & x_{1m} \\ x_{21} & x_{22} & \cdots & x_{2m} \\ \vdots & \vdots & & \vdots \\ x_{n1} & x_{n2} & \cdots & x_{nm} \end{bmatrix} \tag{4}$$

where each x_{ij} is a binary value of either 1 or 0 depending on whether the variable is present or absent in the given voxel.

The key to building a characteristics analysis model is calculating the weight coefficients of the individual variables in the model. Here we define a_j as the weight coefficient of x_j (as outlined above, with j the same in both equations). The coefficient a_j is then calculated using a quadratic sum method based on the assumption that the closer a connection between a given variable (e.g., the voxels of Euclidean distance from the porphyritic diorite in our research area) and another variable (e.g., the voxels of known mineralization in our research area), the more important this first variable is. This means that a_j can be used to measure the relevancy between two variables, here defined as two variables k and j (Zhou and Wang, 2012) as follows:

A. Single matching coefficients are calculated as follows:

$$r_{kj} = \sum_{i=1}^{n} x_{ik}x_{ij} \quad (k,j = 1, 2,\ldots m) \tag{5}$$

where r_{kj} is the matching coefficient between variables k and j. A matching matrix R is then obtained as follows:

$$R = x'x = (r_{kj})_{m\times m} \quad (k,j = 1, 2,\ldots m) \tag{6}$$

B. The next step is to assign values to each variable using a_j ($j = 1, 2, \ldots, m$) to express the relative significance of j in a process that yields a weight coefficient value a_j:

$$a_j = \frac{\sqrt{\sum_{k=1}^{m} r_{jk}^2}}{\sum_{j=1}^{m}\sqrt{\sum_{k=1}^{m} r_{jk}^2}} \quad (j = 1, 2,\ldots,m) \tag{7}$$

The value of a_j indicates the degree of matching between j and k, a value that can be used as the weight coefficient of j.

C. The final step is to calculate connection degree values that reflect the relationship between a given geological body and the area of known mineralization (i.e., training points) within a 3D block model. Here we define "connection degree values" as follows: if we assume that Xujiashan Group contains n voxels: x_i ($i = 1, 2, \ldots, n$), this means that the connection degree value for the Xujiashan Group is the sum of $a_{Xujiashan} \times x_i$. It is generally acknowledged that higher connection degree values reflect more prospective areas, meaning that areas that are highly prospective for mineral exploration can be assessed using these values (Despres, 2004). The connection degree value y_i for n voxels is given using the following formula:

$$y_i = \sum_{j=1}^{m} a_j x_{ij} \quad (i = 1, 2, \ldots,u;\ j = 1, 2, \ldots,m) \tag{8}$$

In a general way, the characteristics analysis method treats geological variables in binary form where "1" indicates the variable is considered highly prospective and "0" means highly unprospective (Botbol et al., 1977; Zhou et al., 2012). This makes characteristics analysis an effective method for prospectivity modeling as it can quantify the relevancy between two geological variables, meaning in turn that the quantitative relevancy of all variables can be normalized with one of these variables assigned a fixed value (e.g., the location of known mineralization – or training points) allowing the calculation of "connection degree values" between this fixed variable and all other variables within the model. The final model superimposes and sums the values of all variables, allowing the identification of highly prospective areas for future exploration (Zhou et al., 2012).

4. Prospectivity modeling and results

The processes outlined above enables the modeling of the 3D prospectivity of areas outside of the known distribution of mineralization within the Yangzhuang deposit. This approach combines 3D geological modeling, 3D spatial analysis, the extraction of factors known to be associated with mineralization, and the construction of a final 3D prospectivity model.

4.1. 3D geological modeling

The Yangzhuang area has sufficient data such as topography, drillhole, cross-section and other geological data to allow the construction of a 3D geological model using GeoVia Surpac™ software. This involved the construction of a drillhole database using the data outlined in Table 1 and the interpretation and extraction of vector files representing geological cross-sections. This was followed by the construction of a 3D contact or boundary model that defines the extent of the research area, the construction of various spatial cross-sections according to the exploration undertaken in the area, and the final restriction and extrapolation of the information within these cross-section using information present within the cross-sections and the drillhole database (Table 1). This then enables the entire study volume to be populated with geological information, the construction of a surface

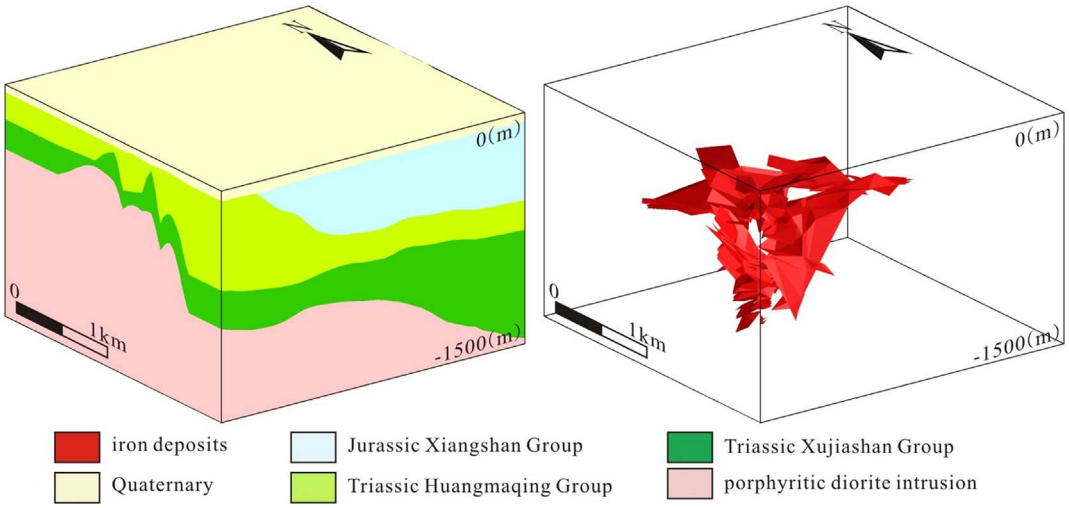

Fig. 8. 3D model of the sedimentary and intrusive units and mineralization within the Yangzhuang area.

model using the built cross-sections and the restriction of these surface models at the top surface of the model using 2D geological modeling. The final step was to combine this surface model with a Boolean operation to construct a final 3D boundary model that includes single geological bodies based on the geological data available from the study area, including sedimentary and intrusive units and the location of known iron mineralization (Fig. 8).

4.2. Extraction of 3D controls on mineralization

The 3D geological model outlined above was used for the 3D spatial analysis and extraction of the key factors associated with mineralization in the study area. This approach used a 3D block model based on the 3D geological model, using a 30 × 30 × 30 m voxel size based on the parameters within the 3D geological model, the known accuracy and precision of the data within the model, and the limitations of the computing system available for this study. This 3D block model contains 337,896 voxels, and solid models were used to restrict the range of the built block model and to populate all of these voxels with values derived from drillhole data. These values were subsequently used for the 3D spatial analysis of the presence or absence of mineralization-related factors within the block model.

The Yangzhuang deposit has been the subject of a significant amount of research during the 1950s, yielding a large volume of geological and geophysical data for this area, as well as identifying the key controls on mineralization in this area (Table 2). These data suggest that the Euclidean distance between key geological units, the uplift and subsidence of the upper surface of the porphyritic diorite and the uplift and subsidence of the upper surface of the Xujiashan Group are all potentially useful guides to mineralization; these 6 predictive variables were extracted from the block models as shown in Fig. 9.

4.3. Characteristic analysis-based 3D prospectivity modeling

The factors extracted above were combined with characteristic analysis to generate a 3D prospectivity model for the study area. This model contains areas of known mineralization and areas that are considered prospective for mineralization, with the former being well characterized and the latter remaining relatively unknown and to be tested during future exploration. This analysis used coding undertaken using Visual Studio 2010 and .NET, yielding a software module that enabled the calculation of weighting coefficients and the computation and visualization of connection degree value with the final output being*.csv property files for each individual block voxel within the model. Areas of known mineralization (i.e., training voxels; Fig. 10) were combined with the 6 variables outlined above to determine the relative importance of these variables in controlling the spatial location of mineralization (i.e., the weighting of these variables). These variables were then used to assess the prospectivity of areas below and peripheral to known areas of mineralization in the study area and to outline key target areas for future exploration.

We statistically analyzed the variables outlined in Table 2 and generated threshold values that delineated the distances where the relationships between these variables and the location of known mineralization broke down. This enabled the identification of prospective and unprospective voxels within our model as follows:

(1) Euclidean distance from the porphyritic diorite and the Xujiashan Group contact: increasing distance from the location of the intrusion is related to a decrease in the spatial relationship between this unit and mineralization (defined using a volume ratio of voxels of known mineralization contained by Euclidean distance from the porphyritic diorite and the Xujiashan Group contact). We assume that prospective voxels are located close to the porphyritic diorite and the Xujiashan Group contact and have a close relationship with known mineralization, so we choose the Euclidean distance whereby the modified porphyritic diorite and the Xujiashan Group contact completely encloses all areas of known mineralization. All voxels of known mineralization are completely contained at a distance of 270 m from the porphyritic diorite and 210 m from the Xujiashan Group (Fig. 11). In addition, we maximized the number of voxels that could be located within this distance to be less than 20% (not including porphyritic diorite and the Xujiashan Group voxels themselves) of the total of 337,896 voxels within the model. We then used the shortest of these distances as the threshold value. Considering 20% of the voxels within the model (with the caveat that the porphyritic diorite contains some 52.4% of the total number of the voxels within the model, meaning that some 72.4% of voxels lie within this threshold) yields a Euclidean distance threshold of 262 m. Combining this with a cell size of 30 m and the fact that 262 m is closer to the original 270 m threshold than 240 m means we choose a value of 270 m as the threshold value (less voxels remain can suppress the interference from the majority of voxels within our model that we consider unprospective), where voxels at distances less than this value are considered prospective in the binary 3D model. In comparison, some 20% of voxels (noting that the Xujiashan Group forms some 21.5% of the voxels within the model, yielding a total amount of 41.5% of the total voxels) lie within a Euclidean distance of 180 m from the Xujiashan Group, with this value used as the threshold during our modeling.

Table 2
Exploration model for Yangzhuang-type iron oxide-apatite deposits.

Controls on mineralization	Name of variables	Use of variable	Generation method
Known mineralization	Known orebody	As training object	Using solid model of the orebody to constrain block model
Ore-bearing lithologies	Sedimentary unit	Euclidean distance from Xujiashan Group	Closely related to ore formation(Fig. 4)	Coding to calculate Euclidean distances
	Mineralized unit	Euclidean distance from porphyritic diorite	The main mineralization-related intrusion is dominated by a porphyritic diorite phase and is associated with more silica-rich porphyritic diorite, porphyritic felsite, spessartine-bearing and gabbroic dikes in the surrounding area	Coding to calculate Euclidean distances
Ore-controlling structures	Doming	Uplift/subsidence of the Xujiashan Group and porphyritic diorite units	Mineralization is generally associated with upright synclines that have NNE–SSW axial trends, extend over a length of 3 km, and have cores that contain Xujiashan Group units	Using average z values to subtract the z value of a given voxel, yielding information on the uplift or subsidence of the voxel in question

(2) Uplift/subsidence of the porphyritic diorite and the Xujiashan Group, where the Feoxide–apatite orebodies in the study area are located in areas that were either uplifted or underwent subsidence during the intrusion of the porphyritic diorite (Fig. 4). Here we present a statistical diagram showing the number of voxels of the porphyritic diorite and the Xujiashan Group that have undergone uplift or subsidence (Fig. 12). This diagram yields inflection points at values of 30 m of uplift and subsidence, separating a small group of voxels with either > 30 m of uplift or < −30 m of subsidence that we consider prospective in our model, suppressing any interference from the majority of voxels within our model that we consider unprospective (Fig. 12).

These binary maps were then combined with connection degree values to compute weight coefficients (Table 3) before these weightings were combined in a 3D model to generate individual weightings for each of the 337,896 voxels in our model, yielding an overall voxel connection degree value. These values range between 0 and 1, with values closer to 1 indicating areas with higher prospectivities; in comparison, values closer to 0 are highly unprospective and should not be considered for future exploration.

We set 99% to be the expected ratio of the total of the 337,896 voxels that should be considered unprospective and a cumulative frequency distribution diagram showing these data is given in Fig. 13. The line y = 334,517 (99% of the total) intersects the original curve at an x value of 0.732. However, the values along X axis are not continuous and the nearest point to 0.6 is actually at 0.742, with this value set to be the threshold for the connection degree value (i.e., the point that discriminates between prospective an unprospective voxels; Fig. 13). We then generated 4 classification diagrams with threshold values of 0, 0.684, 0.724 and 0.742 (each value is an actual connection degree value by calculation rather than a set value or an intersection value), each of which overlap a 2D magnetic anomaly map (Fig. 14). The fact that this magnetic anomaly map is in 2D and cannot be robustly converted to a 3D model means that it is not possible to use these data as a predictive variable and give it a weighting coefficient. However, comparing the 2D magnetic data with the results of our 3D modeling clearly demonstrates that voxels hosting mineralization are associated with 2D mapped areas with magnetic anomaly values > 300 nT, meaning that we use this value as a threshold to discriminate between prospective and unprospective areas (Fig. 14). The areas considered prospective using this magnetic anomaly threshold were combined with their connection degree values to delineate prospective areas in our model. Here, we use Fig. 14D because this model contains sufficient prospective voxels for us to delineate high prospectivity areas and this model contains the least interference from low prospectivity voxels. This modeling outlines three distinct areas of high prospectivity outside of areas of known mineralization that are located to the west (target I), north (target II) and east (target III) of the known mineralization in this region (Fig. 15).

4.4. Results comparison between characteristics analysis and weights of evidence methods

We also generated a weights of evidence model during this study using the same data used for the characteristic analysis approach outlined above in order to cross-compare the results from the two methods. The weights of evidence approach has been successfully used in a range of generally 2D resource assessments and prospectivity modeling projects (Bonham-Carter et al., 1989; Agterberg et al., 1993; Zhang et al., 2009; Wang, 2012; Mao et al., 2013). Here, we outline the basic approach used, which involves the calculation of posterior probabilities based on weights of evidence as follows:

A. The weights of evidence approach uses W^+, W^- and C values, where W^+ is the positive weighting of a given voxel, W^- is the

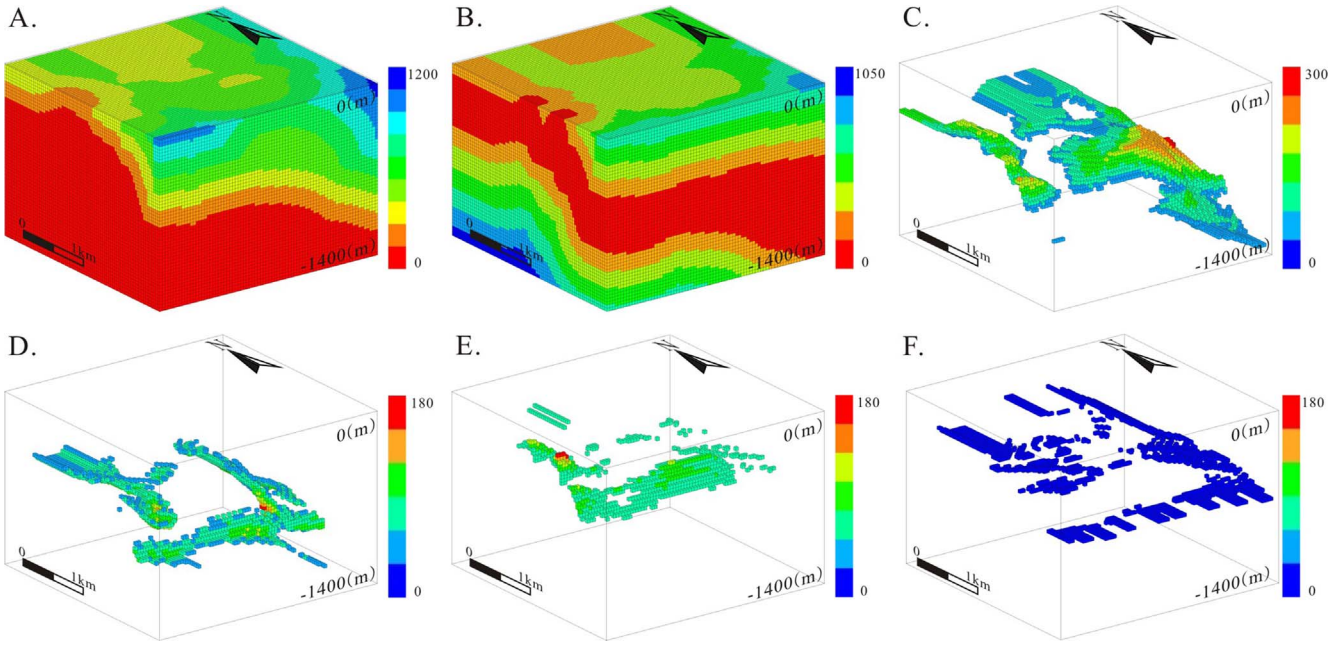

Fig. 9. Block model showing the distribution of the key factors used in the 3D prospectivity modeling undertaken during this study. A = Euclidean distance from the porphyritic diorite, B = Euclidean distance from the Xujiashan Group, C = Uplift of top surface of the diorite intrusion, D = Subsidence of top surface of the diorite intrusion, E = Uplift of top surface of the Xujiashan Group, F = Subsidence of the top surface of the Xujiashan Group.

negative weighting of a given voxel, assuming that several binary patterns can be combined together to predict another binary pattern with W^+ and W^- representing the pair of weights for one single predictor that represent the positive and negative spatial associations between this given predictor and areas of known mineralization. Taking a single predictor pattern, A, the positive weight, W^+ can be expressed as the difference between the unconditional or prior logit of A and the conditional or posterior logit of A, with W^- representing the difference between the prior logit of A and the posterior logit of A, given the absence of another pattern, B (Bonham-Carter, 1994). In addition, C is a contrast coefficient, where positive values indicate voxels that are likely to be prospective for mineralization. We assume that the study area contains t voxels and s of these voxels are associated with known mineralization (i.e., training points), with variable k containing i voxels and n representing the number of intersecting voxels between k and the training points within the model (i.e., areas containing known mineralization), and m indicating the rest of the voxels within the model ($m = i - n$). W^+, W^- and C values that for variable k are indicated by $W_k{}^+$, $W_k{}^-$ and C_k are all calculated using the following formulas (Results are in Table 4):

$$W_k^+ = \ln\frac{n/t}{m/(t-s)} \quad W_k^- = \ln\frac{1-n/t}{1-m/(t-s)} \tag{9}$$

$$C_k = W_k^+ - W_k^- \tag{10}$$

B. Posterior probabilities, or essentially how likely a given voxel is to contain mineralization, were calculated by determining W_{kq} values relating to a given variable k in a given voxel q as follows, assuming that J_q is a Boolean type attribute value of q that has a value of 1 if q is located within k or has a value of 0 if it is located within the subset k:

$$W_{kq} = \begin{cases} W_k^+, (J_q = 1) \\ W_k^-, (J_q = 0) \end{cases} \tag{11}$$

The sum of weights of all variables (F) for a given voxel q assuming there are i variables is calculated as follows:

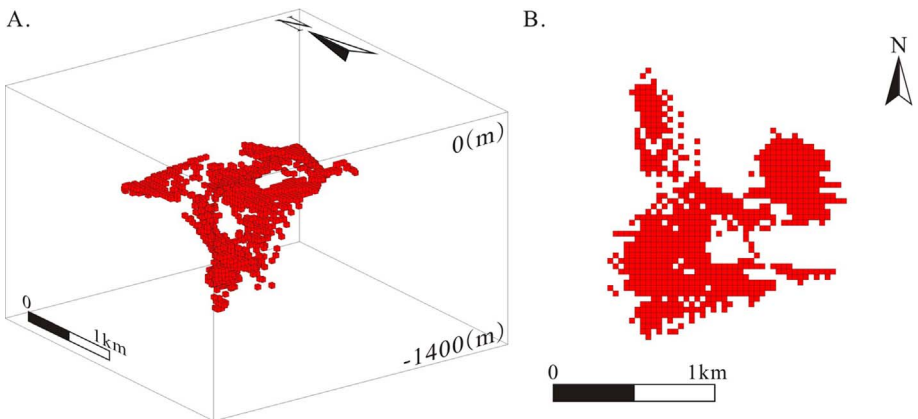

Fig. 10. Block model showing the area of known mineralization (all red voxels in Fig. 10). A = Block model of known mineralization at a dip of 21° and an azimuth of 36°. B = Vertical view of the block model of known mineralization. (For interpretation of the references to colour in this figure legend, the reader is referred to the web version of this article.)

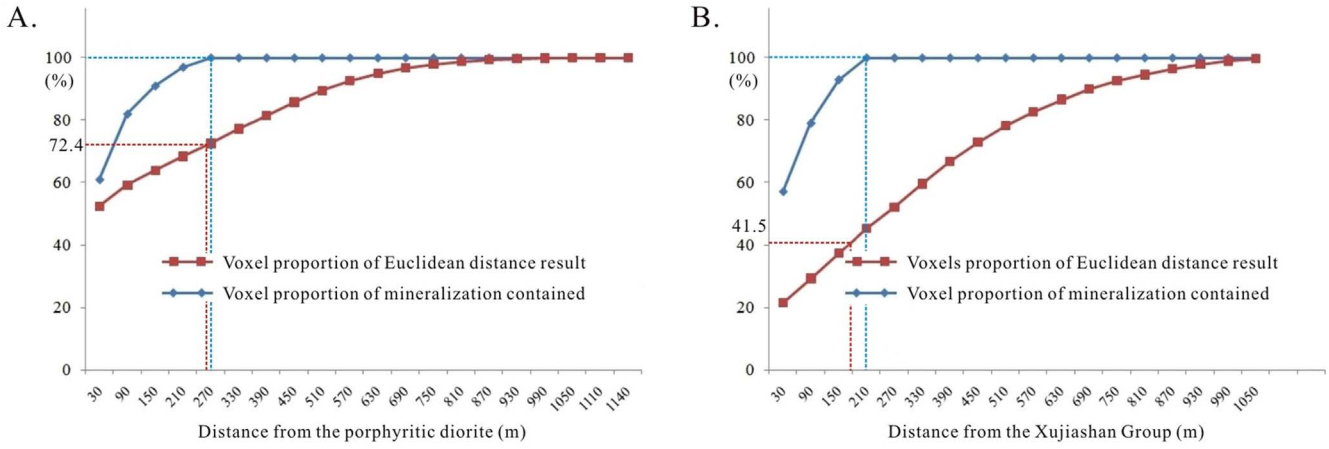

Fig. 11. Cumulative frequency diagrams showing threshold values. A = Cumulative frequency diagram showing the threshold value of the Euclidean distance from the porphyritic diorite (270 m). B = Cumulative frequency diagram showing the threshold value of the Euclidean distance from the Xujiashan Group (180 m).

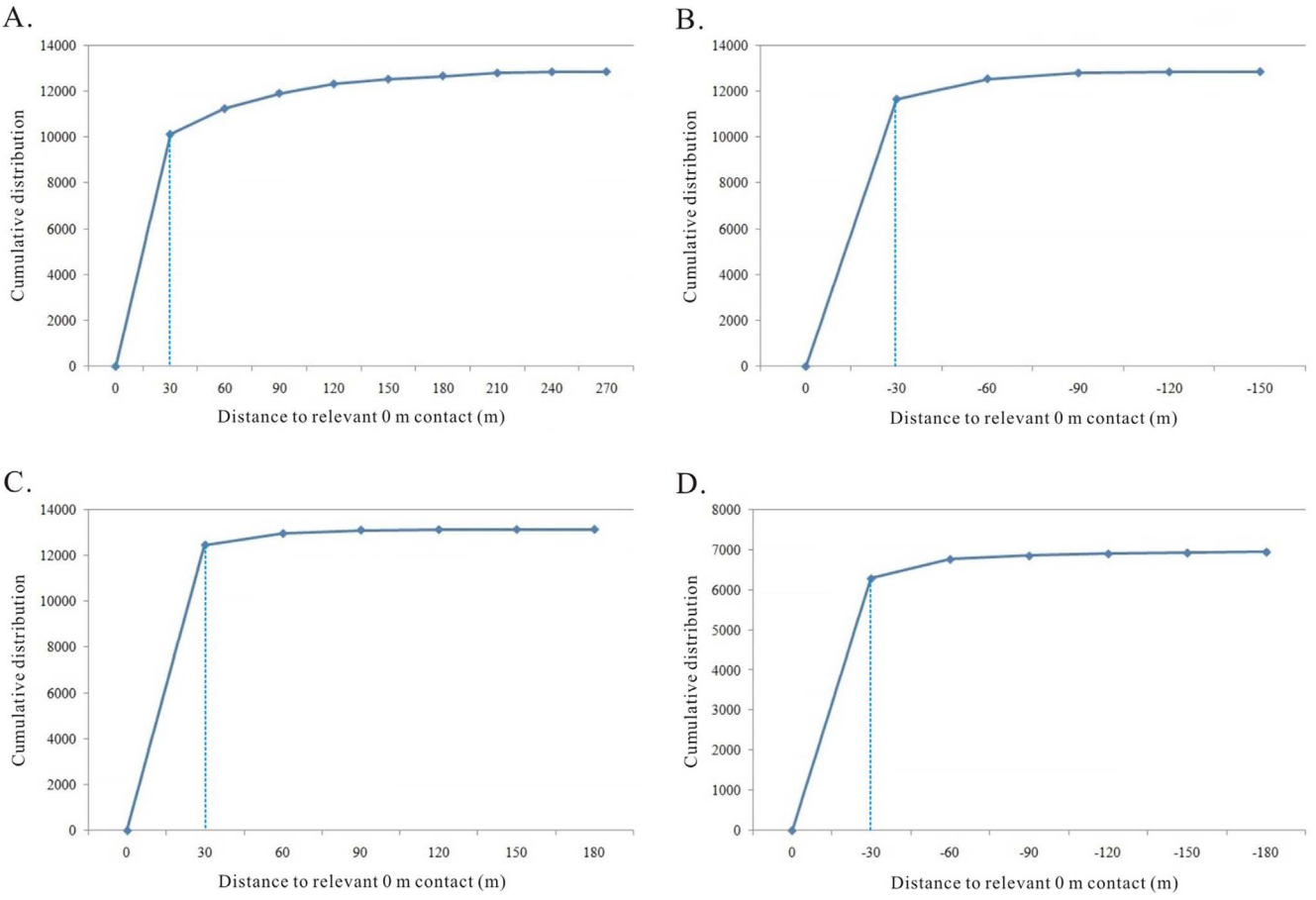

Fig. 12. Cumulative distribution diagram showing the threshold values for uplift and subsidence of the porphyritic diorite and Xujiashan Group surfaces in the study area. A = uplift of the porphyritic diorite, B = subsidence of the porphyritic diorite, C = uplift of the Xujiashan Group, D = subsidence of the Xujiashan Group.

$$F = \sum_{k=1}^{i} W_{kq} \quad (k = 1, 2, 3...i) \tag{12}$$

Finally, the posterior probability of voxel q (here defined as P_q) is calculated using the following formula using the value of F defined in formula (12):

$$P_q = \frac{e^F}{1 + e^F} \tag{13}$$

The weights of evidence derived coefficients suggests that the 3D Euclidean distance from the porphyritic diorite is the most important of the prospectivity factors used during this study in that it is the most closely spatially linked to the known locations of mineralization (with a very high C value of 4.611, where the higher the C value the more closely spatially linked a variable is to the training point dataset). In terms of the other variables, the Euclidean distance from the Xujiashan Group yielded the second highest C value (1.932), and with all other variables having lower values (Table 4). This weights of evidence analysis indicates that the Euclidean distance from the porphyritic diorite is the most important spatial variable in terms of identifying

Table 3
Results of the calculation of prediction variant weighting coefficients undertaken during this study.

Rank	Name	Prospective range (m)	Weighting coefficient
1	Euclidean distance from the porphyritic diorite	0–270	0.315
2	Euclidean distance from the Xujiashan Group	0–180	0.291
3	Uplift of the porphyritic diorite	> 30	0.136
4	Subsidence of the porphyritic diorite	< −30	0.118
5	Uplift of the Xujiashan Group	> 30	0.079
6	Subsidence of the Xujiashan Group	< −30	0.061

areas prospective for mineral exploration, matching the calculated prediction variant weighting coefficients determined using the characteristics analysis method (Tables 3 and 4). Overall, considering both approaches use the exploration model and variables outlined in Section 2.4 and Table 2, these results indicate that a) the variables we have used are associated with the mineralization in the study area and b) that the location of the porphyritic diorite contact is the most important of the mineralization-related variables outlined above.

The weights of evidence coefficients given in Table 4 were used to calculate posterior probabilities and a weights of evidence model. The resulting prospective voxels were then superimposed on the magnetic anomaly data for this area and targets were again identified, yielding a high prospectivity target that is in almost the same location as target I, which was outlined using characteristics analysis and is located to the west of the known area of mineralization. Comparing these results with the results of the characteristics analysis outlined above indicates that the weights of evidence approach did not identify the prospective area to the north (target II of the characteristics analysis approach) and the east (target III of the characteristics analysis approach), both of which are also associated with potentially prospective magnetic anomalies (that were not used during this modeling) within the superimposed magnetic anomaly map. This suggests that although the weights of evidence method can effectively identify some areas that are prospective for exploration outside of the known extent of the Kiruna-type Yangzhuang iron oxide-apatite deposit, the characteristics analysis approach outlined in this study is probably a more effective method for target identification, potentially as this approach can deal more effectively with interdependent data.

We also set 99% to be the expected ratio of the total of the 337,896 voxels that should be considered unprospective and a cumulative frequency distribution diagram showing these data is given in Fig. 16. The line y = 334,517 (99% of the total) intersects the original curve at an x value of 0.051. However, the values along X axis are not continuous and the nearest point to 0.051 is actually at 0.067, with this value set to be the threshold for the posterior probability (i.e., the point that discriminates between prospective an unprospective voxels; Fig. 13). We then generated 4 classification diagrams with threshold values of 0, 0.067, 0.074 and 1 (each value is an actual posterior probability value by calculation rather than a set value or an intersection value), each of which overlaps a 2D magnetic anomaly map (Fig. 17).

The voxels with posterior probability values > 0.067 cover the entirety of the research area, which makes it nearly impossible to delineate targets. As such, we used a value of 0.074 as the threshold value (i.e., Fig. 17C), with the final results shown in Fig. 18.

5. Discussion

Our prospectivity modeling has combined 3D geological information with the location of known mineralization to identify areas that are highly prospective for future mineral exploration around the Yangzhuang deposit in the Zhonggu orefield of the Ningwu Basin of the MLYRMB. Unlike other 3D prospectivity modeling to date, our approach has focused on characteristics analysis (Houlding, 1994; Chen et al., 2007, 2009; Qi et al., 2012; Wang, 2012; Huang, 2013; Li et al., 2014; Yuan et al., 2014a, b;Vollgger et al., 2015; Zhang, 2014) and demonstrates the usefulness of this approach for 3D prospectivity modeling. In terms of targets outside the areas of known mineralization, our targets I and II are associated with the contact between the Xujiashan and Huangmaqing groups at average depths of −390 and −360 m, both of which are coincident with a ≥400 nT geomagnetic anomaly at the surface (Figs. 13 and 14). This target represents the largest high prospectivity region in the study area and as such should be considered the highest priority exploration target in this region (Fig. 14). Target III is associated within the Xujiashan Group, is located at an average depth of −540 m, and is associated with a weaker surficial magnetic anomaly (> 400 nT) that only covers a small area and decreases sharply at the eastern edge of this target area). As such, although all three targets are highly prospective, target III should be considered subsidiary to targets I and II.

The analysis undertaken during this study yielded a series of weight coefficients that enable the statistical identification of the most

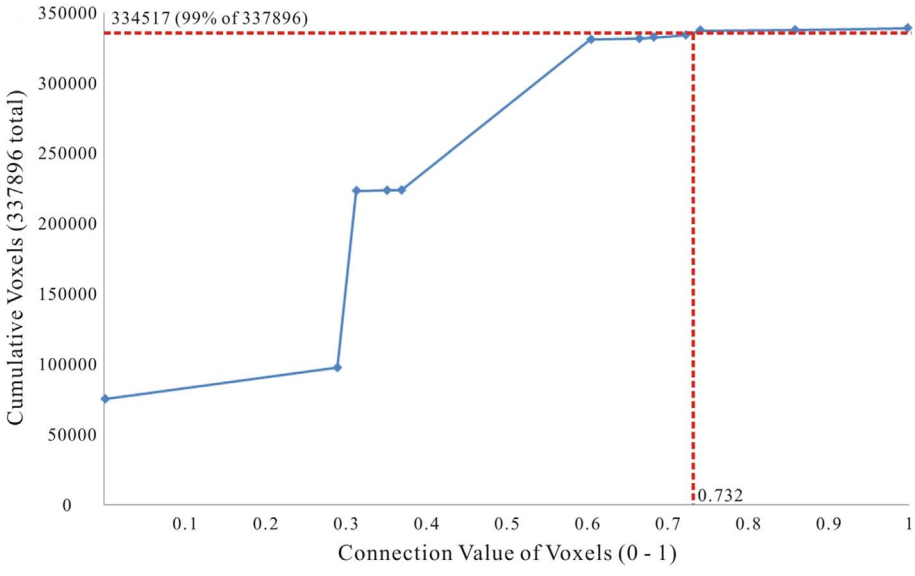

Fig. 13. Cumulative frequency diagram showing variations in connection degree values for all voxels within our prospectivity model.

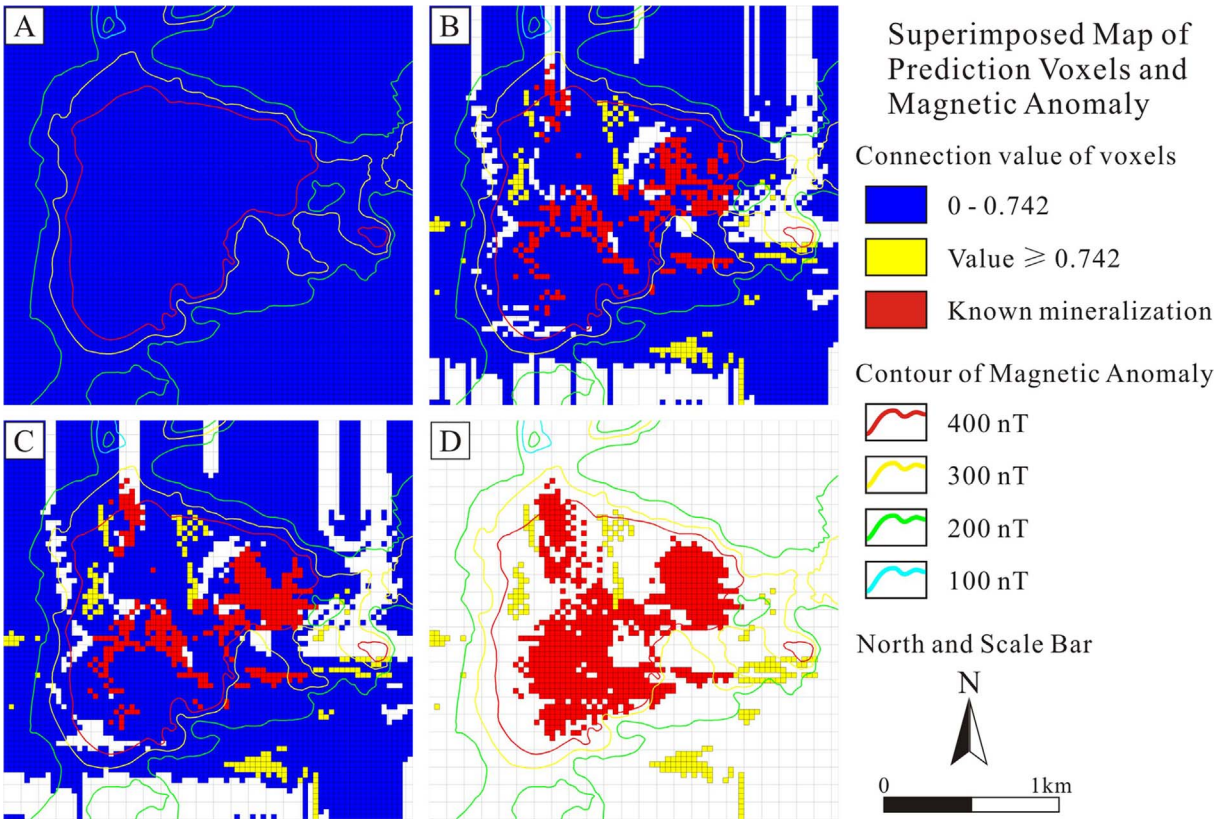

Fig. 14. Classification diagram showing the relationship between voxels carrying prospectivity weightings and a 2D magnetic anomaly map, where voxels are shown in connection degree value terms where values closer to 1 are indicative of areas with higher prospectivities. A = Map showing the distribution of voxels with connection degree values > 0 (i.e., all voxels). B = Map showing the distribution of voxels with connection degree values > 0.684. C = Map showing the distribution of voxels with connection degree values > 0.724. D = Map showing the distribution of voxels with connection degree values > 0.742 (i.e., only voxels that are considered very high prospectivity).

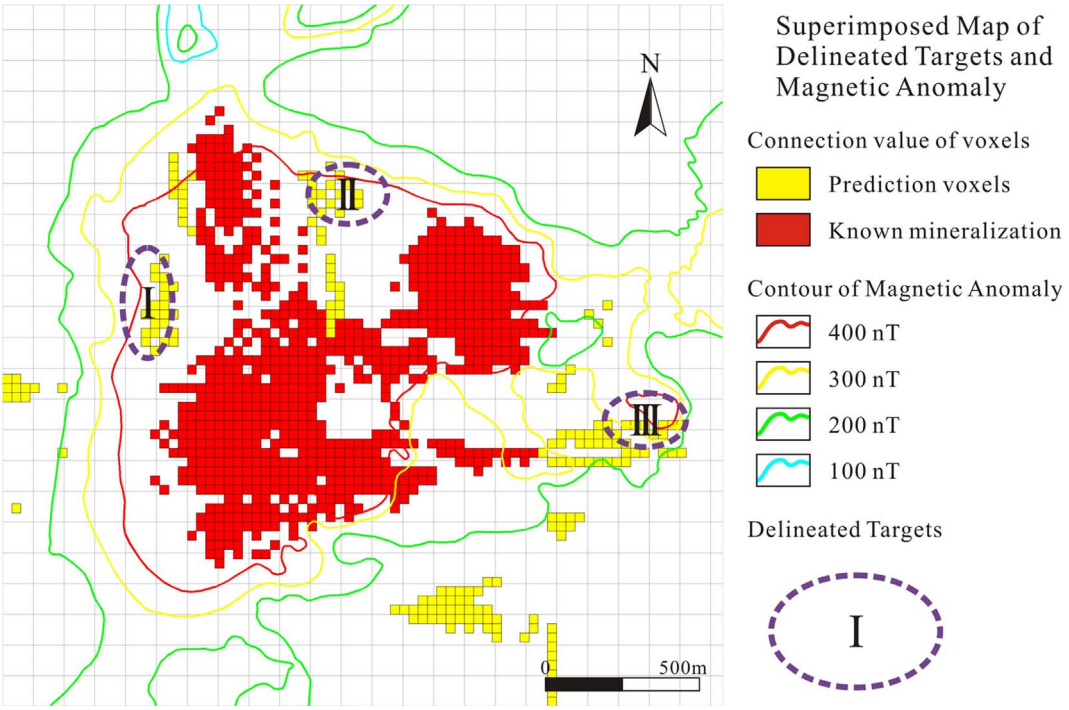

Fig. 15. Results of the 3D prospectivity modeling around the Yangzhuang deposit undertaken during this study shown in terms of connection degree values. These data indicate a good relationship between areas of known mineralization and highly prospective areas but also between highly prospective areas with no currently known mineralization and the extension of the magnetic anomaly associated with the deposit; this is especially clear in the area to the east of the deposit around target III.

Table 4
Weights of evidence based prediction coefficients for the mineralization-related variables used during this study.

Rank	Name	Prospective range (m)	W^+	W^-	C
1	Euclidean distance from the porphyritic diorite	0–270	0.52	−4.09	4.611
2	Euclidean distance from the Xujiashan Group	0–180	0.632	−1.3	1.932
3	Uplift of the porphyritic diorite	> 30	0.955	−0.053	1.008
4	Subsidence of the porphyritic diorite	< −30	0.925	−0.062	0.987
5	Uplift of the Xujiashan Group	> 30	0.498	−0.028	0.525
6	Subsidence of the Xujiashan Group	< −30	0.491	−0.026	0.516

important controls on mineralization in the study area, a key factor in mineral exploration (Buccianti and Esposito, 2004; Table 2). These weighting coefficients indicate that the 3D Euclidean distance from the porphyritic diorite appears to be the most important factor in controlling the location of mineralization (with a weighting of 31.5%), with the Euclidean distance from the Xujiashan Group a close second (29.1%), and with all other variables having lower values (Table 3). This suggests that the porphyritic diorite is the most important control in the location of mineralization in the study area, followed by proximity to the Xujiashan Group. This is unsurprising given the fact that the fluids and metals within the deposits in this area were most likely sourced from the intrusion (Zhou et al., 2008, 2011, 2012) and are concentrated within the intrusion and the Xujiashan Group, with the contact surfaces between these two geological bodies representing a reaction zone that caused the precipitation of ore minerals. This is commonly the case in systems like the one that formed the Yangzhuang deposit as well as others within the MLYRMB and in numerous other magmato-hydrothermal systems such as skarns (e.g., Meinert et al., 2005; Keays and Jowitt, 2013). This clearly demonstrates that (1) the magmatic activity in this area (i.e., the intrusion of the porphyritic diorite) was the key factor in the formation of the mineralization in this area and was most likely the source of the metals and fluids that formed the deposit; (2) the sedimentary unit of the Xujiashan Group are also significant, as they acted as a barrier to the upward ascent of the intrusion, allowing the intrusion to pond and cool down, releasing the fluids that formed the deposit; (3) fractures and contacts between geological bodies (i.e., the contact between the porphyritic diorite and the Xujiashan Group and the contact between Xujiashan and Huangmaqing groups) are also important as these contacts not only may be preferentially fractured, generating space for ore minerals to be deposited, but act as physical and chemical reaction zones that induce the precipitation of ore minerals and the genesis of mineralization. The folded form of the sediments also controlled both the location of the intrusion as well as the deposition of mineralization. All of these factors are known to be important in a wide variety of mineralizing systems as well as the Kiruna-type deposits of the MLYRMB, although the approach here allows the quantification of the relative importance of these factors (as well as the identification of potentially erroneous or misleading parts of exploration models). It appears that the main driving factor of the mineralization in the study area, and maybe mineralization elsewhere in the MLYRMB, is the intrusion of a porphyritic diorite magma. This hypothesis can be tested by using the same approach on similar deposits in the MLYRMB and elsewhere; if this analysis yields very similar results, then it is likely that the main (and only?) control on this type of mineralization may be the presence and potentially the nature (e.g., oxidation state and melt magma composition) of an intrusion. This in turn indicates that future greenfield exploration for this type of mineralization should focus on intrusions, with future brownfield exploration targeting key areas around the intrusion rather than further afield, potentially improving the results of future exploration in this region. These hypotheses need to be tested in future research, although the results presented here clearly demonstrate the value of this type of statistical analysis, not only in terms of exploration targeting but also in terms of furthering our understanding of metallogenic systems. It is also likely that the key relationships identified here may be applicable to other similar mineral systems within the MLYRMB. In addition, the approach used here may create more than just exploration targets if applied to other mineral deposit systems, with the statistical insights associated with the spatial weightings generated using this approach having the potential to identify previously unknown relationships that are key to successful exploration in other areas.

6. Conclusions

(1) This study presents the results of 3D prospectivity modelling for exploration within the area around the Kiruna-type Yangzhuang iron oxide-apatite deposit of the Zhonggu orefield of the Ningwu Basin of the middle-lower Yangtze River Metallogenic Belt using a characteristic analysis based approach. This research suggests that this approach can be used to delineate areas around the

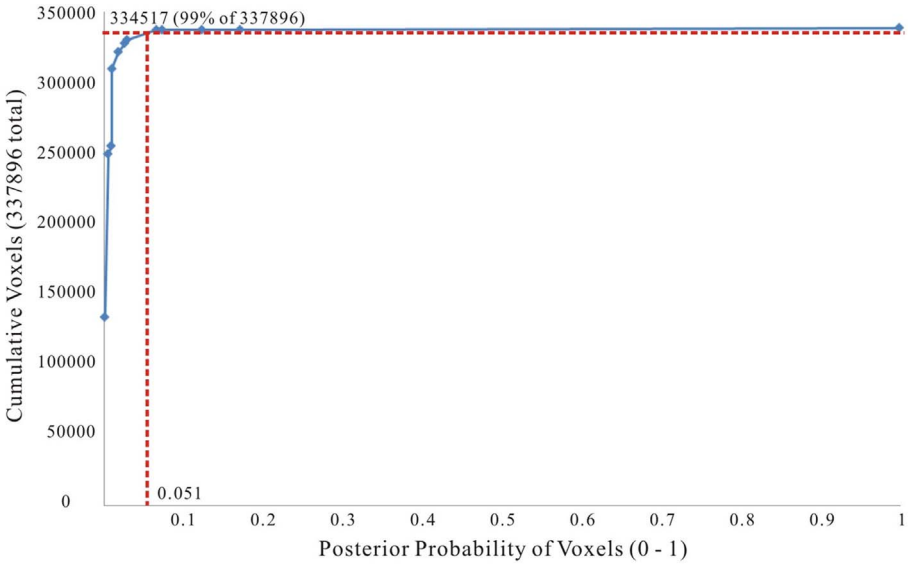

Fig. 16. Cumulative frequency diagram showing variations in posterior probability values for all voxels within our prospectivity model.

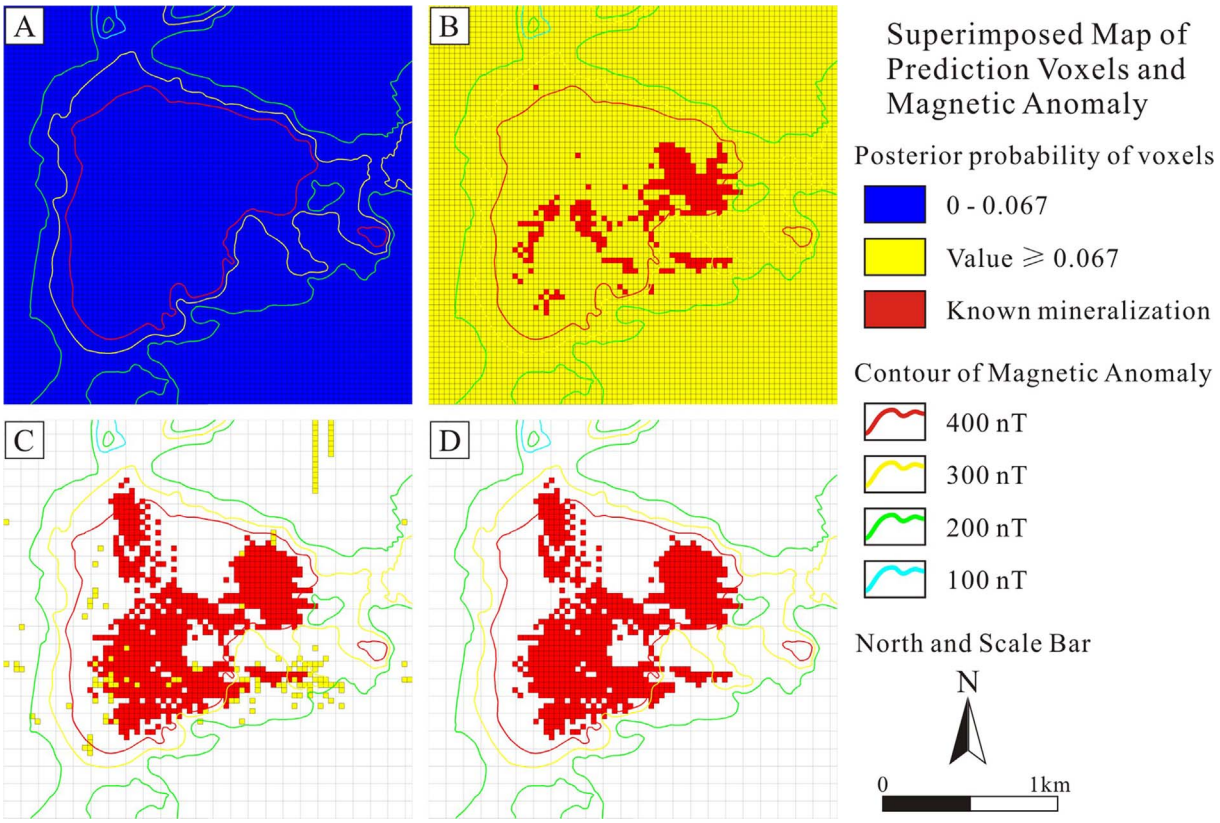

Fig. 17. Classification diagram showing the relationship between voxels carrying posterior probability and a 2D magnetic anomaly map, where voxels are shown in connection degree value terms where values closer to 1 are indicative of areas with higher prospectivities. A = Map showing the distribution of voxels with posterior probability values > 0 (i.e., all voxels). B = Map showing the distribution of voxels with posterior probability values > 0.067. C = Map showing the distribution of voxels with posterior probability values > 0.074. D = Map showing the distribution of voxels with posterior probability values = 1 (i.e., mineralization facts).

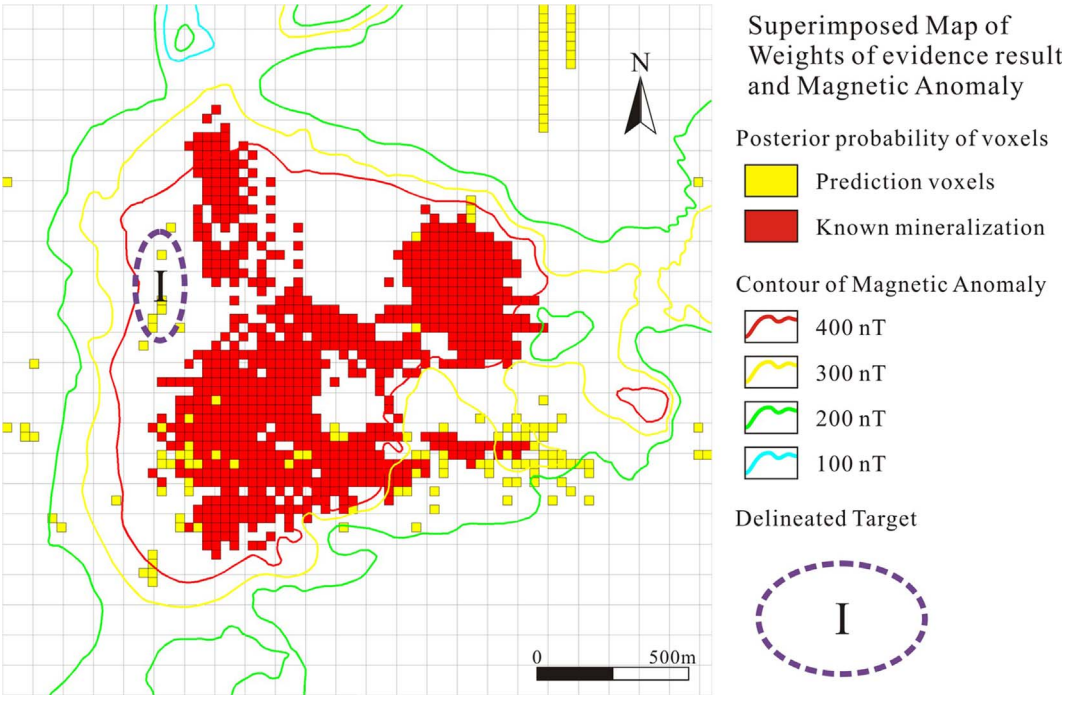

Fig. 18. Results of the 3D prospectivity modeling around the Yangzhuang deposit using weights of evidence method.

Yangzhuang iron deposit that should be considered highly prospective for future exploration. Of the three delineated targets, targets I and II have the highest prospectivities and are associated with distinct magnetic anomalies, suggesting that they should be considered the highest priority for mineral exploration in the Yangzhuang area.

(2) Our research shows that characteristic analysis can be used to generate 3D prospectivity models, and this technique should be

considered for application to other deposit types and other Kiruna-type iron oxide-apatite deposit.

(3) The location of intrusions and the interaction between intrusions and nearby sedimentary unit along contacts between the two (rather than between the sediments themselves) appear to be the main controls on the Kiruna-type Fe mineralization within the study area, a relationship that should be used for exploration both in this area and in other parts of the MLYRMB.

Acknowledgements

This research was financially supported by funds from the National Key R&D Program of China (Grant No. 2016YFC0600209, 2016YFC0600206), the National Natural Science Foundation of China (Grant No. 41702353, 41320104003, 41672069), the Fundamental Research Funds for the Central Universities (Grant No. JZ2016HGTA0710) and the China Academy of Science "Light of West China" Program. We also would like to thank our project partners East China Mineral Exploration and Development Bureau for providing geological data and assistance from the Geological Exploration Technologies Institute of Anhui Province throughout the research. We thank two anonymous reviewers and the handling editor for constrictive comments that improved out manuscript. We also thank Tongke Zheng and Le Shen for their helpful suggestion during the revision of this manuscript and SMJ would also like to thank Billie Pisaniello for assistance during the revision of this manuscript.

References

Agterberg, F., Bonham-Carter, G., Cheng, Q., Wright, D., 1993. Weights of evidence modeling and weighted logistic regression for mineral potential mapping. Comput. Geol. 25, 13–32.

Bonham-Carter, G., 1994. Geographic Information Systems for Geoscientists: Modeling With GIS. Elsevier, Oxford p. 414.

Bonham-Carter, G., Agterberg, F., Wright, D., 1989. Weights of evidence modeling: a new approach to mapping mineral potential. Stat. Appl. Earth Sci. 89, 171–183.

Botbol, J. M., 1971. An application of characteristic analysis to mineral exploration. In: Proceedings of 9th International Symposium on Techniques for Decision-Making in the Mineral Industry, vol. 12, pp. 92–99.

Botbol, J.M., Sinding-larsen, R., Mccammon, R.B., Gott, G.B., 1977. Characteristic analysis of geochemical exploration data. USGS Open File Report: pp. 77–349.

Brown, W.M., Gedeon, T.D., Groves, D.I., Barnes, R.G., 2000. Artificial neural networks: a new method for mineral prospectivity mapping. Aust. J. Earth Sci. 47, 757–770.

Buccianti, A., Esposito, P., 2004. Insights into late quaternary calcareous nannoplankton assemblages under the theory of statistical analysis for compositional data. Palaeogeogr. Palaeoclimatol. Palaeoecol. 202, 209–227.

Chai, F., Yang, F., Liu, F., Santosh, M., Geng, X., Li, Qiang, Liu, G., 2014. The Abagong apatite-rich magnetite deposit in the Chinese Altay Orogenic Belt: a Kiruna-type iron deposit. Ore Geol. Rev. 57, 482–497.

Chang, Y., 1991. The Copper-Iron Belt of the Lower and Middle Reaches of the Changjiang River. Geological Publishing House, Beijing p. 379 (in Chinese).

Chen, J., Lv, P., Wu, W., 2007. A 3D method for predicting blind orebodies, based on a 3D visualization model and its application. Earth Sci. Front. 14, 54–62.

Chen, J., Chen, Y., Wang, Q., 2008. Study on synthetic informational mineral resource prediction using GIS-a case study in Chifeng region, Inner Mongolia, China. Earth Sci. Front. 15, 18–26 (in Chinese with English abstract).

Chen, J., Shang, B., Lv, P., 2009. Large-scale 3D metallogenic prediction of concealed orebody in Gejiu, Yunnan province. Chin. J. Geol. 44, 324–337 (in Chinese with English abstract).

Deng, Z., Lv, Q., Yan, J., Zhao, J., Liu, Y., 2012. The three-dimension structure and the enlightenment to the regional prospecting of the Jiujiang-Ruichang district. Chin. J. Geophys. 55, 4169–4180 (in Chinese with English abstract).

Despres, A.D. 2004. Hydrologic variations between mineral soil flat wetlands, southeastern Virginia. Northeastern Section (39th Annual) and Southeastern Section (53rd Annual) Joint Meeting, Geological Society of America, vol. 36, p. 68.

East China Mineral Exploration and Development Bureau, 2011. Geological Report on the Yangzhuang Deposit, p. 246 (in Chinese).

Gall, B.L., Tiercelin, J.J., Richert, J.P., Gente, P., Sturchio, N.C., Stead, D., Turdu, C.Le., 2000. A morphotectonic study of an extensional fault zone in a magma-rich rift: the baringo trachyte fault system, central Kenya rift. Tectonophysics 320, 87–106.

Hou, T., Zhang, Z., Du, Y., 2010. Deep ore magma-hydrothermal system of Zhonggu ore field in southern part of Ningwu Basin. Earth Sci. Front. 17, 186–194.

Houlding, S.W., 1994. 3D Geosciences Modeling: Computer Techniques for Geological Characterization. Springer-Verlag, California p. 309.

Huang, H., 2013. 3D Geological Modeling and Analysis of Geological Characters of the Hetaoping Pb-Zn Deposit of Baoshan, Western Yunnan. Kunming University of Science and Technology, Kunming p. 81 (in Chinese with English abstract).

Jin, M., 2014. On geological and geochemical characteristics and genesis of iron deposit in Yangzhuang of Dangtu in Anhui. J. Geol. 38, 206–218 (in Chinese with English abstract).

Joly, A., Porwal, A., Mccuaig, T.C., 2012. Exploration targeting for orogenic gold deposits in the Granites-Tanami Orogen: mineral system analysis, targeting model and prospectivity analysis. Ore Geol. Rev. 48 (10), 349–383.

Jowitt, S.M., Cooper, K., Squire, R.J., Thébaud, N., Fisher, L.A., Cas, R.A., Pegg, I., 2014. Geology, mineralogy, and geochemistry of magnetite-associated Au mineralization of the ultramafic–basalt greenstone hosted Crusader Complex, Agnew Gold Camp, Eastern Yilgarn Craton, Western Australia; a Late Archean intrusion-related Au deposit? Ore Geol. Rev. 56, 53–72.

Keays, R.R., Jowitt, S.M., 2013. The Avebury Ni deposit, Tasmania: a case study of an unconventional nickel deposit. Ore Geol. Rev. 52, 4–17.

Li, X., Yuan, F., Zhang, M., Jia, C., Zhou, T., Zhang, S., Zheng, T., Gao, D., Hong, D., Liu, X., 2014. 3D localization and quantitative prospectivity mapping Ysing artificial neural networks: a case study of the Baixiangshan Mining Area, Ningwu Basin. Acta Geol. Sin. 88, 644–656 (in Chinese with English abstract).

Li, X., Yuan, F., Zhang, M., Jia, C., Jowitt, S.M., Ord, A., Zheng, T., Hu, X., Li, Y., 2015. Three-dimensional mineral prospectivity modeling for targeting of concealed mineralization within the Zhonggu iron orefield, Ningwu Basin, China. Ore Geol. Rev. 71, 633–654.

Lv, P., Bi, Z., Zhu, P., Sun, Y., Chen, J., 2011a. The development of some important simulation techniques for geosciences. Geol. Bull. China 31, 677–682 (in Chinese).

Lv, Q., Shi, D., Tang, J., Wu, M., Chang, Y., SinoProbe-03-CJ Research Group, 2011. Probing on deep structure of middle and lower reaches of the Yangtze Metallogenic BELT and typical ore concentration area: a review of Annual Progress of SinoProbe-03. Acta Geosci. Sin. 32, 257–268 (in Chinese with English abstract).

Mao, X., Tang, Y., Lai, J., 2011. Three dimensional structure of metallogenic geologic bodies in the Fenghuangshan ore field and ore-controlling geological factors. Acta Geol. Sin. 85, 1507–1518 (in Chinese with English abstract).

Mao, X., Zou, P., Cao, F., Hu, C., Zhang, B., Zhou, S., 2013. GIS-based extended weights of evidence method based on linear regression in metallogenic prognosis. Sci. Surv. Mapp. 38 (3), 18–21 (in Chinese with English abstract).

Mao, X., Zhang, M., Deng, H., Zou, Y., Chen, J., 2016. Three-dimensional visualization prediction method for concealed ore bodies in deep mining areas. J. Geol. 40 (3), 363–371 (in Chinese with English abstract).

Mccammon, R.B., Botbol, J.M., Sinding-Larsen, R., Bowen, R.W., 1983. Characteristic analysis—1981: final program and a possible discovery. J. Int. Assoc. Math. Geol. 15 (1), 59–83.

Meinert, L.D., Dipple, G.M., Nicolescu, S., 2005. World Skarn Deposits. 100th Anniversary Volume Economic Geology pp. 299–336.

Ni, Z., Xue, Q., 2007. Application of Quantitative Characteristics Analysis in Metallogenic Prediction. Science and Economy in Inner Mongolia, 132, 117–118 (in Chinese with English abstract).

Ningwu Research Group, 1978. Ningwu Porphyry Iron Ores. Geological Publishing House, Beijing p. 197 (in Chinese).

Porwal, A., Carranza, E.J.M., 2015. Introduction to the Special Issue: GIS-based mineral potential modelling and geological data analyses for mineral exploration. Ore Geol. Rev. 71, 477–483.

Porwal, A., Gonzalez-Alvarez, I., Markwitz, V., McCuaig, T., Mamuse, A., 2010. Weights-of-evidence and logistic regression modeling of magmatic nickel sulfide prospectivity in the Yilgarn Craton, Western Australia. Ore Geol. Rev. 38, 184–196.

Porwal, A., Das, R.D., Chaudhary, B., et al., 2015. Fuzzy inference systems for prospectivity modeling of mineral systems and a case-study for prospectivity mapping of surficial Uranium in Yeelirrie Area, Western Australia. Ore Geol. Rev. 71, 839–852.

Qi, G., Lv, Q., Yan, J., Wu, M., Liu, Y., 2012. Geologic constrained 3D gravity and magnetic modeling of Nihe deposit-a case study. Chin. J. Geophys. 55, 4194–4206 (in Chinese with English abstract).

Song, Y., Yang, T., Zhang, H., Liu, Y., Hao, H., Li, Z., 2015. The Chaqupacha Mississippi valley-type Pb–Zn deposit, central Tibet: ore formation in a fold and thrust belt of the India–Asia continental collision zone. Ore Geol. Rev. 70, 533–545.

Tang, Y., 1998. Geology of Copper-Gold Polymetallic Deposits in the Along-Changjiang Area of Anhui Province. Geological Publishing House, Beijing p. 351 (in Chinese).

Vollgger, S.A., Cruden, A.R., Ailleres, L., Cowan, E.J., 2015. Regional dome evolution and its control on ore-grade distribution: insights from 3D implicit modelling of the Navachab gold deposit, Namibia. Ore Geol. Rev. 69, 268–284.

Wang, X., 2012. Study on 3D Mineral Prospectivity Prediction in Baixiangshan Deposit Based on Weights of Evidence Method. Publishing House of Hefei University of Technology, Hefei p. 51 (in Chinese with English abstract).

Wang, Y., Zhang, Q., Wang, Y., 2001. Geochemical characteristics of volcanic rocks from Ningwu area, and its significance. Acta Petrol. Sin. 17, 565–575 (in Chinese with English abstract).

Wu, C., Xu, D., Zhou, Y., Hou, M., Yu, L., Hu, G., 2015. Metallogenic prognosis for Skarn-type deposits based on characteristic analysis in Southern Hainan Island. Geotectonica et Metallogenica 39, 528–541 (in Chinese with English abstract).

Yoshinobu, A.S., Okaya, D.A., Paterson, S.R., 1998. Modeling the thermal evolution of fault-controlled magma emplacement models: implications for the solidification of granitoid plutons. J. Struct. Geol. 20, 1205–1218.

Yuan, F., Zhou, T., Liu, J., Fan, Y., Cooke, D.R., Jowitt, S.M., 2011. Petrogenesis of volcanic and intrusive rocks of the Zhuanqiao stage, Luzong Basin, Yangtze metallogenic belt, east China: implications for ore deposition. Int. Geol. Rev. 53, 526–541.

Yuan, F., Li, X., Zhang, M., 2014a. Three dimension prospectivity modelling based on integrated geoinformation for prediction of buried orebodies. Acta Geol. Sin. 88, 630–643 (in Chinese with English abstract).

Yuan, F., Li, X., Zhang, M., Jowitt, S.M., Jia, C., Zheng, T., Zhou, T., 2014b. Three-dimensional weights of evidence-based prospectivity modeling: a case study of the

Baixiangshan mining area, Ningwu Basin, Middle and Lower Yangtze Metallogenic Belt, China. J. Geochem. Explor. 145, 82–97.
Zhai, Y., 1992. Metallogenic Regularity of Iron and Copper (Gold) Deposits in the Middle and Lower Valley of the Yangtze River. Geological Publishing House, Beijing p. 255 (in Chinese).
Zhang, M., 2014. 3D Mineral Prospectivity Prediction in Zhonggu Ore Fields, Ningwu Basin. Publishing House of Heifei University of Technology, Hefei p. 147 (in Chinese with English abstract).
Zhang, S., Cheng, Q., Zhang, S., Xia, Q., 2009. Weighted weights of evidence and stepwise weights of evidence and their application in Sn-Cu mineral potential mapping in Gejiu, Yunnan Province, China. Earth Sci. J. China Univ. Geosci. 34, 281–286 (in Chinese with English abstract).
Zhang, D., Zhou, Y., Wan, Y., Song, H., 2012. Application of characteristics analysis to optimization of prospective area of mineral deposits. J. Sichuan Univ. Sci. Eng. (Natural Science Edition) 25, 93–96 (in Chinese with English abstract).
Zhao, P., 1983. Deposit Statistic Prediction. Geological Publishing House, Beijing p. 314 (in Chinese).
Zhao, P., 2003. Quantitative Geoscience: Methods and Its Applications. Higher Education Press, Beijing p. 464 (in Chinese with English abstract).
Zhao, P., Chen, J., 2000. Prospect of mineral resources economics in the 21st century. J. Nat. Resour. 15 (3), 197–200 (in Chinese with English abstract).
Zhao, Z., Tu, G., 2003. Super-Large Ore Deposits in China(II). Science Press, Beijing p. 631 (in Chinese).
Zhou, Y., Wang, Z., 2012. Mathematical Geoscience. Sun Yat-sen University Press, Guangzhou p. 247 (in Chinese).
Zhou, T., Fan, Y., Yuan, F., 2008. Advances on petrogenesis and metallogeny study of the mineralization belt of the Middle and Lower Reaches of the Yangtze River area. Acta Petrol. Sin. 24, 1665–1678 (in Chinese with English abstract).
Zhou, T., Fan, Y., Yuan, F., Zhang, L., Ma, L., Qian, B., Xie, J., 2011. Petrogensis and metallogeny study of the volcanic basin in the Middle and Lower Yangtze Metallogenic Belt. Acta Geol. Sin. 85, 712–730 (in Chinese with English abstract).
Zhou, T., Fan, Y., Yuan, F., Zhong, G., 2012. Progress of geological study in the Middle-Lower Yangtze River Valley metallogenic belt. Acta Petrol. Sin. 28, 3051–3066 (in Chinese with English abstract).